Chemical Engineering Journal 452 (2023) 139125

Contents lists available at ScienceDirect

Chemical Engineering Journal

journal homepage: www.elsevier.com/locate/cej

Kinetic model for Pd-based membranes coking/deactivation in propane dehydrogenation processes

Camilla Brencio [a], Robin Gough [a], Anouk de Leeuw den Bouter [a], Alba Arratibel [b], Luca Di Felice [a], Fausto Gallucci [a,c,*]

[a] Sustainable Process Engineering, Department of Chemical Engineering and Chemistry, Eindhoven University of Technology, De Rondom 70, Eindhoven 5612 AP, the Netherlands
[b] Membrane Technology and Process Intensification / Materials and Processes, TECNALIA, Basque Research and Technology Alliance (BRTA), Mikeletegi 2, San Sebastian, Spain
[c] Eindhoven Institute for Renewable Energy Systems (EIRES), Eindhoven University of Technology, PO Box 513, Eindhoven 5600 MB, the Netherlands

ARTICLE INFO

Keywords:
Membrane deactivation
Propane dehydrogenation
Hydrogen permeation
Pd membranes

ABSTRACT

This work aims at providing insight into the deactivation mechanism of Pd-based membranes in propane dehydrogenation processes. Thermogravimetric analysis (TGA) experiments were conducted to study the adsorption and coking of propylene over conventional thin layer (TL) and double-skinned (DS) Pd-based membranes under several operating conditions. A mechanistic monolayer-multilayer coke growth model was selected to mathematically describe the membrane coking observed during TGA experiments. In addition, the reaction rate of coke formation and its influence on membranes deactivation has been studied. The deactivation model able to describe the hydrogen flux decay over time suggests that monolayer coke is the main responsible for the membrane deactivation. Multilayer coke also causes deactivation but with a smaller order than monolayer coke, for both the TL and the DS membranes. Among the two membrane types, DS membrane deactivates faster, i.e. with a higher order than the TL membrane, which is equal to 1.55 for the former and 0.51 for the latter. This is related to the higher number of active sites available in the controlling step of the deactivation reaction, which are most probably given by the addition of the ceramic Al_2O_3 protective layer. XPS spectra further confirms that, in the presence of Pd, Al_2O_3 sites contribute to carbon formation by evidencing a different nature of carbon formed on the two membranes. Finally, the experimental results of hydrogen permeation over time conducted on different membranes types and operative conditions confirmed the validity of the derived and parametrized kinetic models for coke formation and membrane deactivation. The experimental findings and the kinetic model derived in this work provide essential tools for the design and optimization of membrane reactors for dehydrogenation processes.

1. Introduction

Palladium-based membrane technology has gained significant attention for its application in dehydrogenation processes [1–4]. Combining the catalytic activity of Pd atoms with theoretically infinite hydrogen perm-selectivity, Pd and Pd alloy membranes are commonly used for ultra-pure hydrogen production and to increase the yield of equilibrium limited reactions with the removal of H_2 from reaction mixtures [5–8]. The dehydrogenation (DH) processes, which main drawbacks are due to the endothermic-equilibrium limited main dehydrogenation reactions, have the potential to become more energy efficient and economically attractive when the membrane reactor technology with integrated Pd-based membranes is used. The continuous removal of hydrogen from the reaction ambient by membrane separation increases the DH conversion at a given temperature. This in turn would allow for a lower operating temperature keeping the same conversion/yield, which consequently reduces the downstream separation efforts. The lower operating temperature will help mitigating another drawback of DH processes, which is the high rate of coke formation on the catalyst occurring at high temperatures. The use of the H_2-selective membrane inside the reactor would not only improve the yield of the main dehydrogenation reaction, but it would also improve the

* Correspondence author.
E-mail address: F.Gallucci@tue.nl (F. Gallucci).

https://doi.org/10.1016/j.cej.2022.139125
Received 12 July 2022; Received in revised form 26 August 2022; Accepted 6 September 2022
Available online 10 September 2022

efficiency of the downstream separation section. This would result in bigger advantages than simply using the H_2-selective membranes in the downstream separation section. For this reason, numerous research activities in the field of process intensification are related to membrane reactors [9]. Didenko et al. [10] carried out an experimental work on the dehydrogenation of propane in a combined membrane reactor. In their work, they have demonstrated, at laboratory scale, the potential of the membrane reactor technology in increasing the feedstock conversion to propylene by a factor of 1.6–2.0 with respect to the conventional equilibrium value, under optimized operating conditions. Ricca et al. [11] investigated a novel process scheme for the production of propylene via propane dehydrogenation, where the dehydrogenation reaction unit is integrated with a Pd-based membrane for the recovery of hydrogen. The results show that the presence of the membrane assured an increasing propane conversion along the system, allowing values above thermodynamic conversion of a traditional unit without membranes. Such solution enables for a better stability of the catalyst, and accordingly a prolonged operation time without need for catalyst regeneration. Another interesting work that investigates the use of the membrane reactor technology for dehydrogenation processes is presented by He et al. [12]. In this work, the authors performed a thermodynamic analysis of a novel solar driven propane dehydrogenation system with a membrane reactor. The results shown that compared to the performance of a traditional reactor (without membranes), an H_2 permeate pressure of 5–10 bar increases the conversion rate of C_3H_8 from 4.1 % to 99.12 % and the selectivity of C_3H_6 from 93.1 % to 99.1 % at 400 °C. Thus, the membrane reactor has the potential to significantly increase the dehydrogenation reaction yield at lower temperatures via H_2 separation utilization. In comparison with other common hydrogen separation methods (i.e. pressure swing adsorption, solvent adsorption, cryogenic techniques), membrane separation technologies possess economic benefits by reducing operational costs, decreasing energy consumption and minimize the amount of unit operations [13]. When looking into membranes that can be used for hydrogen separation, dense membranes show higher selectivity towards hydrogen than porous ones. The selectivity towards hydrogen in porous membranes actually increases when the hydrogen flux is relatively low, which is of course not desired for industrial scale situations [14]. For the same reason, dense metallic membranes are preferred compared to dense ceramic and polymeric membranes for the purpose of high-purity hydrogen separation. To selectively separate hydrogen with a dense membrane, a metal surface is needed to have both a potential energy surface strong enough to dissociate hydrogen and the ability to dissolve hydrogen. A number of metallic elements in group 10 (i.e. nickel, palladium and platinum) have been proven to have the ability to dissociate and dissolve hydrogen, as do some metals in groups 3–5. However, only palladium has shown an exceptional solubility of hydrogen in the bulk metal (Pd can reversibly absorb up to 935 times its own volume of hydrogen), resulting in a superior ability to transport hydrogen [13].

However, the application of Pd-based membranes in dehydrogenation processes is limited by the presence of short chain hydrocarbons and carbon side-products, which may negatively affect the hydrogen flux stability through the membrane over time. Carbon-based components tend to adsorb on the membrane surface and subsequently dissociate, leading to membrane coking (carbonaceous deposits on the surface), which inhibits the hydrogen adsorption and dissociation, thus reducing its flux [15–19]. Several authors have recently studied the permeance inhibition of conventional Pd-alloyed membranes in the presence of light hydrocarbon mixtures. Montesinos et al. [15] analyzed the effects of the composition of propane/propylene mixtures on the hydrogen permeation through commercially available dense Pd-Ag membranes supported on porous stainless steel. The experimental results reported in this work reveal that propylene leads to a significant transient decrease in H_2 permeation due to its decomposition. Carbon deposits cover the Pd/Ag membrane layer, leading to membrane deactivation. Haw Jung et al. [20] investigated the hydrogen permeation through a palladium disk membrane (5 mm in diameter and 50μ m in thickness) in the presence of steam, methane, propane and propylene. Results shown that methane and propane have only a negligible effect on hydrogen permeance, but propylene strongly decreases hydrogen permeance especially at higher temperatures. Peters et al. [21] tested the hydrogen flux through conventional unsupported thin Pd-Ag and Pd-Cu alloy films, applying representative propane dehydrogenation gaseous feed mixtures under different operating conditions. The experimental results confirmed that coke formation is very likely under the operating conditions required for an integrated catalyst and membrane system, i.e., temperatures of 450–500 ℃ and low hydrogen to propene ratios. Carbon formation is inevitable during dehydrogenation processes, leading to the inhibition of the activity of both the catalyst particles and the membranes with similar deactivation rates. The large rate of coke formation during dehydrogenation processes limits continuous operation in an integrated membrane reactor. However, the use of H_2-selective membranes integrated in the reaction unit can mitigate this phenomenon, lowering the operating temperature and thus the rate of carbon formation. Since the membrane coking has been demonstrated to be reversible through regeneration with diluted oxygen, the membrane reactor technology can be successfully used to improve the performance of dehydrogenation processes.. A kinetic model able to describe accurately the behavior of the membrane reactor system under a variety of operating conditions could help in the design and optimization of the most suitable reactor configuration. Although the dehydrogenation reaction has been widely studied, most of the works only focus on the deactivation of the catalysts produced by coke formation, with lack of information regarding the deactivation of the Pd-based membrane modules.

The aim of this work is to provide insight into the deactivation mechanism of Pd-based membranes under propane dehydrogenation process applications. We present a mechanistic kinetic model for the coke formation and its influence on the deactivation of Pd-based membranes, which is key for further improvement of these membranes' formulation, as well as an essential tool for reactor and process design. First, thermogravimetric analysis (TGA) experiments were conducted to study the adsorption and coking behaviour of propylene over Pd-based membranes under several operating conditions. The deactivated membranes were characterized using X-ray photoelectron spectroscopy (XPS) analysis, to study the nature of the deposited carbonaceous species. Then, the reaction rate of coke formation has been derived to mathematically describe the membrane coking observed during TGA experiments. Finally, the influence of the coke formation reaction rate on the membrane deactivation and hydrogen flux reduction has been studied. The detail model of the carbon formation rate on membranes paves the way for a more realistic transient reactor model for the design of the dynamic membrane assisted propane dehydrogenation.

2. Materials and methods

2.1. Pd-based membranes

In this work, the adsorption behavior of propylene has been investigated on the top selective layer of two different Pd-alloyed membrane types. The membranes are prepared by the co-deposition of the selective Pd-Ag membrane on a porous tubular substrate made of Al_2O_3, using the electroless plating technique, following the procedure described in detail in the work of Arratibel et al. [22]. The resulting membranes are denoted as conventional Pd-Ag membranes. Furthermore, an additional mesoporous layer made of YSZ/γ-Al_2O_3 has been deposited on top of the Pd-Ag layer by a vacuum-assisted dip coating technique [23]. This leads to a different membrane type, denoted as double-skinned Pd-Ag membrane.

TGA samples were prepared by detaching the top selective layer from the porous support. This was done by cutting the membrane layer(s) along the direction of the tube with a diamond cutting wheel and peeling

off the layer from the porous support. The protective layer of the double-skinned configuration has been analyzed separately, to gain more insight on its specific contribution on carbon deposition and ultimately on the performance differences between the two membranes. This sample was tested in powder form. To obtain the powder representative of the protective layer, the corresponding YSZ/γ-Al_2O_3 sol mixture, characterized by a total concentration of ceramic equal to 1.5 wt% with a mass ratio of 50 wt% YSZ and 50 wt% boehmite and prepared according to the procedure reported by Arratibel at al. [24], was firstly dried and then calcinated at 550 ℃ with a heating rate of 1 ℃/min, for 3 h in air. The main specifics of the different samples analyzed in this work are summarized in Table 1.

2.2. Thermogravimetric system

Coke formation experiments were performed in a thermogravimetric system (TGA), schematically represented in Fig. 1. The system uses a microbalance, model MK2-5 M from CI-Precision, with a sensitivity of 0.1 μg and a maximum capacity of 5 g and +/- 500 mg operating range. The balance head is kept at constant temperature, and it is continuously purged with a constant N_2 flow (0.5 l_{STP}/min) to prevent reactive gas mixtures entering the balance. The balance is attached to a porous basket (0.5 cm d × 1.5 cm l), made of Al_2O_3, with a loading capacity between 20 and 50 mg. The basket is positioned inside the reactor, consisting of a ceramic tube of 15 mm in diameter. The reactor is in turn placed inside a SS shell, surrounded by an electrically heated oven to maintain isothermal conditions. The reactor temperature is controlled using a thermocouple positioned close to the sample to ensure stable conditions. The process gases are regulated by Bronkhorst mass flow controllers and fed from the bottom of the TGA system.

The experiments were conducted with a total feed flow rate of 0.5 l_{STP}/min, at atmospheric pressure and varying the temperature from 355 to 450 ℃ (at these conditions absence of mass transfer limitations have been assessed with separate experiments). The following procedure has been adopted to perform carbon formation experiments: first, the sample is heated up under a N_2 flow; once the operating temperature is reached, it is exposed to a pure propylene feed and the resulting weight increase is ascribed to carbon deposition. At the end of the experiment the empty basket was exposed to air at high temperatures of 800 ℃ for 2 h, to clear it from possible carbon traces present on its surface. As a blank test, each experiment was firstly performed on the empty basket, following the same procedure reported above. This is done to remove the buoyancy forces of the feeding gases and to eliminate the effect of carbon deposition on the basket and wire, if any. Weight measurements, collected every 5 s, have been analyzed to retrieve the carbon content

Table 1
Specifics of the different samples studied in this work.

Sample	Sample ID	Composition [wt%]	Type	Sample weight TGA [mg]	Sample surface area TGA [cm^2]
Protective layer	PL	50 YSZ-50 Al_2O_3	Powder	46	–
Conventional thin selective layer	TL	96.6 Pd-4.23 Ag *	Layer	44	3.25
Double-skinned protective & selective layer	DS	50 YSZ-50 Al_2O_3 93.3 Pd-Ag 6.7 *	Layer	44	3.25

* The composition of the selective layer was determined by measuring the concentration of both metals in the plating bath before and after deposition of the layer, using an ICP-OES technique.

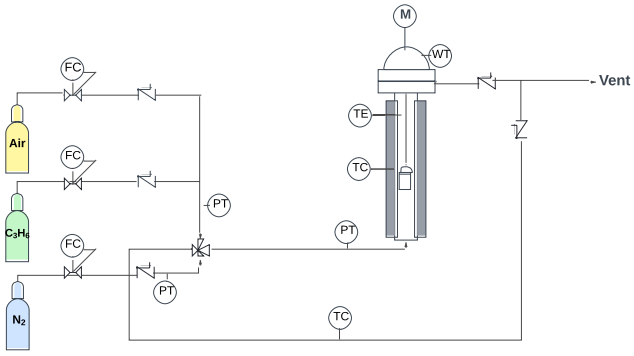

Fig. 1. Schematic representation of the TGA setup. FC indicates mass flow controllers, TI and TC represent thermocouples and controllers, respectively. PT indicates pressure transducers. M indicates the microbalance. WT indicates the weight transmitter.

per unit of sample measured, according to the following expressions:

$$\Delta W = W(t) - W\left(t_{f,\ cycle\ 2}\right) \quad (1)$$

$$\text{Carbon content} = \frac{\Delta W_{sample} - \Delta W_{empty\ basket}}{W_{sample}} \left[\frac{mg_{carbon}}{mg_{sample}}\right] \quad (2)$$

To fit the coke formation kinetic expression, the TGA results have been expressed per unit of surface area of membrane tested, in cm^2 (reported in Table 1). This is done to represent in a more realistic way the mechanism of carbon formation that occurs on the surface area of the membrane selective layer. The total amount of coke that can form on a membrane is only related to the surface area which is exposed to the coke precursor, regardless of the membrane selective layer thickness and thus the amount present (expressed in weight).

To assess the absence of mass transfer limitations under the selected operating conditions, a series of experiments were conducted varying the sample mass, from 48 mg to 21 mg, and the total feed flow rate, from 0.5 to 4 l_{STP}/min. The results obtained for this set of experiments are reported in Appendix A1.

2.3. XPS measurements

Conventional ultrahigh vacuum XPS was performed using a K-Alpha XPS spectrometer, supplied by Thermo Scientific. The samples were placed on a double-sided carbon tape, and then transferred into the analysis chamber of the XPS machine at room temperature. The chamber was evacuated with two 260 L/s turbo molecular pumps to reach ultra-vacuum (base pressure kept in low 10–8 mbar range). Spectra were collected using monochromatic Al K alpha X-rays at 1486.568 eV, running at 72 W and a spot size of 400μ m. The spectra were acquired using the flood-gun source to account for surface charging. All the spectra were then analyzed using the CasaXPS software. Before analysis of the data, the binding energy data was referenced to the C 1 s line (284.8 eV) for charge correction. The spectra were deconvoluted using a symmetric pseudo-Voigt function, referred to as GL(30) and GL(10) in CasaXPS software, after subtracting the Shirley background.

2.4. Fitting procedure and model discrimination

The fitting procedure was performed with MATLAB® R2019b. The kinetic parameters were determined via the *lsqnonlin* optimization procedure, based on the well-known Levenberg-Marquardt algorithm [25]. Given a set *m* of observations of the form (x_i, y_i), this algorithm determines the vector of parameters $\hat{\beta}$ for the model $f(x_i, \beta)$ which minimizes the residual sum of squares $RSS(\beta)$ as follow:

$$RSS(\beta) = \text{argmin}_{\beta} \sum_{i-1}^{m} [y_i - f(x_i, \beta)]^2 \quad (3)$$

The same fitting routine has been used firstly to fit thermogravimetric experiments to different coke formation models; then, the best kinetic model obtained was used to calculate the effect of coke formation on the membrane deactivation. This is done by fitting the experimental hydrogen flux, obtained during permeation tests performed in a previous work by the same authors, to the hydrogen flux expression corrected by different expressions for the membrane activity-coke relationship. To determine the optimum parameters for the transient coke formation model, the algorithm minimizes the sum of squares of the difference between the concentrations of coke determined over time experimentally and via the model prediction, respectively, expressed per unit of sample tested in mg_{coke}/cm^2_{sample}. The optimized parameters of the membrane deactivation model are then obtained by minimizing the sum of squares of the difference between the flux of hydrogen determined over time experimentally and via the model prediction, respectively, expressed in $mol/s/m^2$.

The selected *lsqnonlin* algorithm requires an initial guess for the fitting parameters and most importantly, lower (LB) and upper (UB) boundaries, to keep the fitted parameters in a reasonable range. The *lsqnonlin* algorithm requires a good initial guess for the fitting parameters to converge to a reasonable fit. To avoid the strong dependence of this fitting routine from the initial guess, the *MultiStart* build-in function of MATLAB is used [26]. This function runs the *lsqnonlin* optimization procedure 20 times with a tolerance set equal to 10^{-6}, starting every time from a different vector of initial guesses automatically selected among the lower and upper boundaries. The final solution identified by the *MultiStart* function corresponds to the initial guess for which the optimization algorithm gives the best solution, which minimized the residual sum of squares RSS. To further increase the robustness of the optimized parameters, an additional routine is implemented to run the optimization algorithm in a loop, with a lower tolerance (equal to 10^{-10}) and using the newly obtained results as initial guess, until the squared norm of the residual of the last iteration is equal to the one of the previous iteration.

To find the most reasonable model among those proposed in this work, different indicators describing the goodness of the fit have been considered. The first indicator is represented by the outcome of the fitting routine used, which is the sum of square residuals corresponding to the differences between the experimental and calculated values (Eq. (3)). An additional indicator used in this work is the Akaike Information Criterion (AIC) [27]. This indicator can be used for least squares parameters estimation, according to literature [28,29]. The AIC indicator considers both the number of parameters p each model has to fit and the residual sum of squares (RSS), according to the following formula:

$$AIC = 2p - 2\ln(L) \quad (4)$$

where p is the number of parameters of the tested model and $\ln(L)$ is the numerical value of the log-likelihood at its maximum point. This value can be calculated in the case of a nonlinear fit with normally distributed errors, using the residuals from the nonlinear least-squares fit RSS_{opt} and their number n as reported below:

$$\ln(L) = 0.5\left(-n(\ln(2\pi) + 1 - \ln(n) + \ln\sum_{i=1}^{n} RSS_{opt}\right)\right) \quad (5)$$

AIC includes the number of model parameters and therefore it avoids over-parametrization, penalizing models with a higher number of parameters to be fitted. This indicator is calculated for each model considered and the model with the lowest absolute value of AIC is chosen as the best. To make the comparison easier to interpret, the so called Akaike weight of model i is calculated as follows [30]:

$$w_i(AIC) = \frac{e^{-0.5\,\Delta_i(AIC)}}{\sum_{k=1}^{K} e^{-0.5\,\Delta_k(AIC)}} \quad (6)$$

where $\Delta_i(AIC)$ describes the difference between model i and the model with the lowest AIC value, while K represents the overall number of the models compared. The sum of all the w_i gives 1. This indicator indicates the weight of evidence of the model to describe the underling mechanism among the set of models analysed.

Finally, the 95 % confidence intervals were determined to evaluate the quality of the fit. Two different methods are used to calculate the confidence intervals. For the best parameters of the coke formation model, the bootstrapping algorithm is used [31,32]. The confidence intervals for the best parameters of the deactivation model are determined using the nlparci function in MATLAB.

2.5. Kinetic expressions for coke formation and deactivation models

In this work, well known kinetic models reported in literature for the catalysts used in dehydrogenation applications have been reviewed and used as basis for the carbon formation on the membrane surface. This is because the membrane H_2-selective material (Pd) acts as a catalyst for the hydrogen splitting, while the protective layer material in the DS (Al_2O_3) is also known to be active in coke formation and thus can be treated as a catalyst.

The coke formation models considered in this work are all based on the Monolayer-Multilayer Coke Growth Model (MMCGM) [33,34]. According to this model, it is possible to distinguish two different contributions of coke formed on the catalyst surface, known as monolayer (C_m) and multilayer (C_M) coke respectively, where C indicates the concentration of monolayer/multilayer coke expressed in mg_{coke}/mg_{sample}. This model considers coking to start directly on the active sites present on the surface of the catalyst to form the monolayer coke. Subsequent coking can either form on the new active sites or on the primary layer to form the secondary layer, known as multilayer coke, leading to a simultaneous deposition of layers. Both types of coke will cause the filling of active metal sites for PDH leading to deactivation and their relative concentrations depend on the reactions leading to their formation [35]. The total amount of coke formed over time (t) is given by the sum of the two contributions, as expressed in Eq. (4) and (5):

$$C = C_m + C_M\left[\frac{mg_{coke}}{mg_{sample}}\right] \quad (7)$$

$$r_C = \frac{dC_c}{dt} = \frac{dC_m}{dt} + \frac{dC_M}{dt}\left[\frac{mg_{coke}}{mg_{sample}min}\right] \quad (8)$$

According to the MMCGM, the formation of monolayer coke includes the adsorption of the reactant/product on the catalyst surface, the formation of the coke precursor and the consequent coke formation. The rate of monolayer coke formation is proportional to the fraction of active sites available on the catalyst surface, and it is calculated from Equation (6).

$$r_{C_m} = \frac{dC_m}{dt} = k_{1c}(C_{max} - C_m)^h\left[\frac{mg_{coke}}{mg_{sample}min}\right] \quad (9)$$

Where k_{1c} is the kinetic constant of the monolayer-type coke formation, C_{max} is the maximum coke concentration in the monolayer, expressed in mg_{coke}/mg_{sample}, and h describes the reaction order of the monolayer coke growth. The order h is representative of the number of sites involved in monolayer coke formation step. A value of h equal to 1 indicates that the coke formation step involves only one active site. When $h = 2$, then it means that the monolayer coke formation step involves two sites on the active catalyst surface [33,36,37].

The rate of formation of multilayer coke can be described by Eq. (7).

$$r_{C_M} = \frac{dC_M}{dt} = k_{2c} C_m^n \left[\frac{mg_{coke}}{mg_{sample} min}\right] \quad (10)$$

Where k_{2c} is the kinetic constant of the multilayer coke growth and n describes the reaction order of the multilayer coke growth. The multilayer coke grows on top of the previously existing coke and thus it is proportional to the fraction of sites covered on the monolayer, with a kinetic order of formation equal to n. A value of n equal to 0 is representative of a constant activity of the multilayer coke [33,36,37]. A value of n equal to zero predicts a constant activity of the multilayer coke, meaning that monolayer coke does not necessarily need to reach the equilibrium ($C_m = C_{max}$) to ensure that multilayer coke formation starts [38].

The kinetic constants of the monolayer and the multilayer coke growth k_{1c} and k_{2c} aredescribed by the Arrhenius Equation (Eq. (8)), as follow:

$$k_{ic} = k_{ic,0} \exp\left(\frac{E_{ia}}{R}\left(\frac{1}{T} - \frac{1}{T_0}\right)\right) \qquad \text{with } i = 1, 2 \quad (11)$$

where $k_{ic,0}$ is the preexponential factor, E_{ia} is the activation energy in J/mol, R is the universal gas constant in J/(mol K), T is the temperature and T_0 is the reference temperature, expressed in Kelvin. The reference temperature is calculated as an average of the three experimental temperatures investigated and it is equal to 405 ℃.

Depending on the values of the reaction orders of the monolayer and the multilayer coke growth, it is possible to mathematically derive different expressions of the MMCGM. Table 2 summarizes different integrated forms of the MMCGM known from literature and tested in this work (C1 to C5). Beside the expressions already reported in literature, an additional approach which assumes that the total coke formation corresponds only to the monolayer coke growth contribution is here proposed (C6).

To link the membrane deactivation trends, observed over time during hydrogen-propylene permeation tests, with the coke content on the membrane, different models able to describe the transient deactivation term a are considered. The deactivation term is combined with the hydrogen flux expression through Pd-based membranes, according to the following equation:

$$J_{H_2}(t) = a\, J_{H_2,\,1D} \quad (18)$$

where $J_{H_2,\,1D}$ is the hydrogen flux through Pd-based membranes described by a one-dimensional steady state model, expressed in mol/(s m^2). This term accounts for concentration polarization and other mass transfer limitations in the retentate side of the membrane and does not account for coke formation and deactivation. This model has been presented in another work by the same authors [41]. By multiplying the steady state hydrogen flux expression $J_{H_2,\,1D}$ with the dimensionless transient deactivation term a, it will be possible to describe the hydrogen flux decay over time $J_{H_2}(t)$ representative of the membrane deactivation trend. The models able to describe the transient deactivation term a have been already proposed in literature to correlate the activity a with coke content in catalysts. The coke-activity relationship is generally expressed by potential (Eq. (16)-(17)) or exponential (Eq. (18)) equation forms. Table 3 summarizes different expressions for the activity-coke relationship known from literature [33,34] and considered in this work (D1 to D5). In those expressions, the parameters α_1 and α_2 are proportionality factors which indicate the contribution that the monolayer and multilayer coke have towards deactivation. The deactivation order *m* is related to the relationship between the coke formation and the deactivation trend [40]. In the case of membrane deactivation, a higher deactivation order means that the drop in H_2 flux is more severe upon coke formation. Typical values of *m* reported in literature for dehydrogenation catalysts range between 1 and 2. When $m = 1$, the activity would decrease linearly with coke coverage, while if $m = 2$, a straight line would be derived from the plot of the square root of the activity versus coke content [38]. Among all the proposed deactivation models, D1 considers that catalyst activity depends on active sites in the catalyst surface and thus its deactivation is only due to the coke formed in the monolayer. Models D2 and D3 link the deactivation of the catalyst to both the coke formed in the monolayer and in the multilayer. Models D4 and D5 assume as well that multilayer coke also deactivates the catalyst, but this coke is considered to have additional catalytic activity. This leads the catalyst to have a residual activity even after its surface has been covered by coke [39]. This explains the plus term present in the right side of equations Eq. (19) and (20). Among all the deactivation models listed in Table 3, we decided not to test models D4 and D5, where the catalyst is assumed to have a residual activity even after the surface has been covered by coke. This observation is not suitable for Pd-based membranes, since hydrogen permeation through them follows seven elementary steps reported below [42,43]:

a. Diffusion of molecular hydrogen to the surface of the membrane
b. Adsorption and decomposition in atoms on the Pd-allow surface

Table 3
Expression for the membrane activity-coke relationship.

Model ID	m	Model Equation	Eq.	Ref
D1	2	$a = (1 - \gamma_1 C_m)^m$	(20)	[39]
D2*	m	$a = (1 - \gamma_1 C_m - \gamma_2 C_M)^m$	(21)	[40]
D3	–	$a = \exp(-\gamma_1 C_m - \gamma_2 C_M)$	(22)	[40]
D4	–	$a = (1 - \gamma_1 C_m) + \gamma_2 \left(\frac{C_m}{C_m + C_M}\right)$	(23)	[39]
D5	–	$a = (1 - \gamma_1 C_m) + \gamma_2 C_m e^{-\gamma_3 (C_M / C_m)}$	(24)	[39]

* m is treated as an additional free parameter during the fitting routine.

Table 2
Integrated forms of the monolayer-multilayer coke growth model (Eq. (5)-(7)) for different reaction orders.

Model ID	h	n	Model Equation	Eq.	Ref
C1	1	1	$C_c = C_{max}\left[\frac{k_{1c} - k_{2C}}{k_{1c}}\right] + k_{2c} C_{max}\, t$	(12)	[38–40]
C2	2	0	$C_c = C_{max}^2 \left[\frac{k_{1c} t}{1 + C_{max} k_{1c} t}\right] + k_{2c} t$	(13)	[38–40]
C3	2	1	$C_c = C_{max}^2 \left[\frac{k_{1c} t}{1 + C_{max} k_{1c} t}\right] - \frac{k_{2c}}{k_{1c}} \ln[1 + k_{1c} t C_{max} t] + k_{2c} C_{max} t$	(14)	[38–40]
C4	1	0	$C_c = C_{max}(1 - e^{-k_{1c} t}) + k_{1c}\, t$	(15)	[28]
C5*	h	0	$C_c = C_{max} - \left((h-1) k_{1c} t + C_{max}^{1-h}\right)^{\frac{1}{1-h}} + k_{2c} t$	(16)	[28]
C6*	h	–	$C_c = C_{max} - \left((h-1) k_{1c} t + C_{max}^{1-h}\right)^{\frac{1}{1-h}}$	(17)	–

* h is treated as an additional free parameter during the fitting routine.

c. Atomic hydrogen transition from Pd-alloy surface to Pd-alloy bulk
d. Diffusion in the Pd-alloy bulk
e. Atomic hydrogen transition from Pd-alloy bulk to Pd-alloy surface
f. Recombination of hydrogen atomic and desorption on the Pd-alloy surface
g. Diffusion of molecular hydrogen from the surface of the membrane

According to this mechanism, hydrogen needs firstly to adsorb on the Pd-surface to permeate though Pd-based membranes. Thus, once the Pd-alloy surface is completely covered by coke, there are no more active sites for the hydrogen to adsorb and then permeate and the membrane cannot have a residual activity for hydrogen permeation. This is also confirmed by experimental results of hydrogen permeation under propylene exposure. The hydrogen flux through the Pd-based membranes has a continuous decreasing trend over time. Based on those considerations, only models D1 to D3 (reported in Table 3) have been tested in this work to find the best relationship between coke formation and membrane deactivation.

3. Results

3.1. Coke formation on Pd-based membranes

Thermogravimetric analysis (TGA) experiments were conducted to study the coking behavior of Pd-based membranes as function of time. According to the results obtained by the same authors during permeation tests on Pd-based membranes under both propane and propylene mixtures, propylene is identified to be the main coke precursor. The experimental results show stable performance of Pd-based membranes under propane exposure; the paraffins adsorb on the membranes surfaces with no further decomposition to carbon species and the membrane can restore immediately the initial hydrogen flux as soon as the alkane is removed from the mixture [41]. Therefore, TGA experiments were performed to study the adsorption behavior of propylene over Pd-based membranes, with temperatures between 355 ℃ and 450 ℃, at atmospheric pressure. Fig. 2(a) and 2(b) illustrate the coking behavior as function of time at different operating temperatures, for the conventional thin selective layer (TL) and the double-skinned top layer (DS) samples respectively.

For the two different samples tested, it is possible to make some common considerations on the carbon formation behavior. The trend of carbon concentration over time follows two main stages. Firstly, carbon formation is characterized by a sharp increase (sharp zone) within the first 10 min. Then, it follows a more moderate linear increase (linear zone) during the rest of exposure to propylene. The difference between the two zones is more evident at higher operating temperatures. Similar results have been already observed for dehydrogenation catalysts by Gascon et al., Pena et al. [38], Lobera et al. [39] and van Sint Annaland et al. [44]. The presence of two zones with different trends for the coke concentration over time would suggest that coke deposition itself causes the deactivation of the coking reaction rate, being faster in the sharp zone and slower in the second linear zone, where a residual coking activity remains. As expected, larger carbon formation is observed at higher operating temperatures. This observation is in line with the more severe deactivation trend of hydrogen flux registered during permeation tests as the operating temperature is increased [17,21,41]. From here, it is possible to conclude that the rate of coking increases with temperature. Comparing the coking behavior of the conventional and the double-skinned membranes, it is evident that the coke concentration of the DS sample is always higher than that in the TL sample. This difference is even more pronounced for higher operating temperatures. The two samples differ due to the presence of the additional mesoporous ceramic protective layer on top of the selective one, in the case of the DS sample.

TGA experiments were conducted on the raw protective layer (PL) sample in powder form. As shown in Fig. 3, coke formation is detected on the PL sample, which is expected due to the well-known activity of Al_2O_3 acid sites [45]. The higher coke concentration on PL compared to the TL and DS samples is believed to be related to the higher surface area offered by its powder form – while the TL and the DS samples have been tested under the form of layers. Further analysis of the DS sample was done to analyze the contribution of the protective layer on the overall coke formation. Knowing the total weight of DS sample tested, the thickness of the protective layer from fabrication specifics, and the total density and volume of the protective layer from BET results, it was possible to calculate the weight percentage of the protective layer (PL) on the total DS sample. According to the calculations, the weight

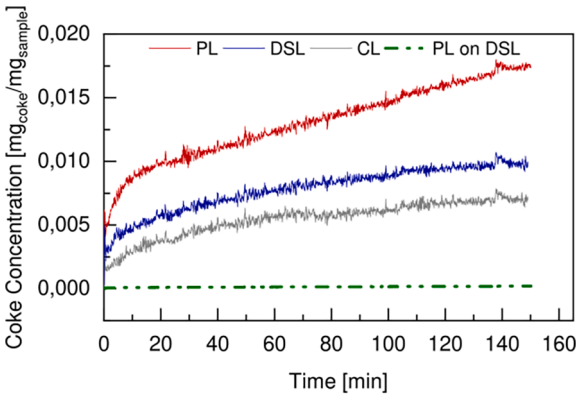

Fig. 3. Coke concentration over time at 410 ℃, for the protective layer (PL), the conventional selective layer (CL), the protective layer (b) and the double-skinned top layer (DS) and the protective layer on the double-skinned sample (PL on DS), under exposure to 0.5 l_{STP}/min of 100 vol% C_3H_6 at atmospheric pressure.

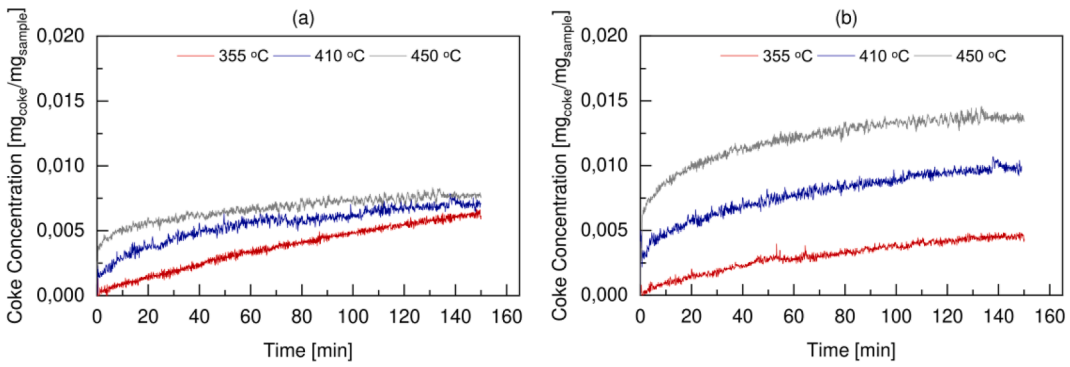

Fig. 2. Coke concentration over time at 355, 410 and 450 ℃, for the conventional thin selective layer (a) and the double-skinned top layer (b) samples, under exposure to 0.5 l_{STP}/min of 100 vol% C_3H_6 at atmospheric pressure.

fraction of the protective layer on the DS sample resulted to be equal to 1.2 wt%, while the remaining 98.8 wt% is represented by the selective (PdAg) layer. By normalizing the coke content registered on the PL sample (expressed in $mg_{coke}/mg_{PL\ sample}$) with the weight percentage of protective layer present on the DS sample (expressed in $mg_{PL\ sample}/mg_{DS\ sample}$), it was possible to retrieve the effective contribution of the protective layer on the double-skinned sample.

It was found that the amount of coke on the protective layer was negligible in comparison to the amount of coke formed on the rest of the DS sample, even under the overestimating assumption that the protective layer would be as reactive as in powdered form. This indicates that the increase in carbon formation observed in the DS is the effect of the coexistence and cooperation of Pd and Al_2O_3 sites instead of the sum of two independent catalytic routes.

3.2. Coked membranes characterization

To further study the surface chemical composition of the carbonaceous species deposited on the Pd-based membranes samples tested in TGA, X-ray photoelectron spectroscopy (XPS) analysis was used and compared to the results reported in literature [46–50]. A high-resolution scan of the C1s region for both the conventional thin layer and the double-skinned membrane samples is reported in Fig. 4a and 4b, respectively. The C1s XPS spectra were fitted according to the procedures already reported in literature [46,51].

The C1s XPS spectra of the TL sample can be deconvoluted into three C—C peaks: the C—C primary peak at 284.1 eV is attributed to sp^2 hybridized carbon and indicates the presence of aromatic and graphitic carbon in the C_xH_y [49]. The other two peaks, which are the C—C low at 283.2 eV and the C—C high at 284.8 eV, are instead attributed to sp^3 hybridized carbon. Those peaks indicate the presence of defective and contaminated carbon, meaning C in cyclopentane, cycloheptene or larger rings with clusters [5152]. An additional peak is present in the C1s spectra of the TL sample at higher binding energy, which is the so-called $\pi - \pi^*$ (HOMO-LUMO) peak at 287.4 eV [51]. This is a transition peak for carbon in aromatic compounds coming from the ring excited by exiting photoelectrons, with a characteristic shape- up line [47]. Looking at the C1s XPS spectra of the DS sample, it is possible to identify again the three C—C peaks present also in the TL sample: the primary C—C peak at 284.08 eV, the C—C low peak at 283.5 eV and the C—C high peak at 285 eV. However, the C1s spectra of the DS sample shows an additional peak centered at a higher binding energy (288.4 eV), which is not present in the C1s spectra of the TL sample. This is an oxygen containing peak and it is deconvoluted into two peaks [50,51]. The first one, the C═O peak, is centered at 287.9 eV and is representative of carbonyl groups (C═O) and carbon linked to two ether/hydroxyl bounds (O—C—O). The second COO peak is positioned at 288.4 eV and it indicates carboxyl groups (COOH) and primary carbon in lactone/ester groups (COOC) [51]. The three C—C peaks are present on both the TL and the DS samples in similar concentrations, while the C═O and the COO peaks are only present in the DS sample, as shown in Table 4.

As the sample was not exposed to oxygen, the oxygen that leads to the formation of C═O and COO groups indicated by the XPS spectra can only come from the alumina present on the protective layer on top of the selective one in the DS sample. The same observation has been reported by other authors. Sarbak et al. [53] investigated the nature of carbonaceous deposits formed during the conversion of hydrocarbon by infrared spectroscopy (IR). The FTIR spectrum reported in their study indicates two characteristic IR bands at 1575 and 1462 cm^{-1}, representative of carboxylate groups. According to the authors, the formation of carboxylate from the hydrocarbons indicates that the oxygen is provided exclusively by alumina [54]. Vu et al. [55] investigated the location and structure of coke generated over Pt–Sn/Al_2O_3 in propane dehydrogenation. The authors report the XPS spectra of both the fresh and the spent catalyst used for propane dehydrogenation; in both cases, the C1s spectrum is composed of a peak representative of oxidized carbon in carboxyl groups O-C═O, which is attributed to the oxygen present on the alumina support. It is inferred that the additional peaks present in the DS sample and representative of carbonyl compounds are related to the coexistence of the ceramic Al_2O_3 protective layer and Pd in the selective one, resulting in the higher carbon content observed in the DS sample than in the TL one during TGA experiments.

3.3. Coke formation kinetics

Tables 5 and 6 report the information required for the model discrimination procedure described in Section 2.4 for the conventional and the double-skinned membranes. Among the different models tested for the description of carbon formation on Pd-based membranes, model C5 is the most representative for our system since it shows the lowest value of RSS, and it has the highest Akaike weight regardless of its additional free parameter h. The kinetic parameters obtained from the fitting procedure for model C5 are reported in Table 6, for both the conventional thin layer (TL) and the double-skinned (DS) membranes.

As already observed by Pena et al. [38], values for activation energy

Table 4
Peak deconvolution results for XPS spectra of the TL and DS samples.

	Peak Position [eV]		Area		Concentration [%]	
	TL	DS	TL	DS	TL	DS
C—C low	283.3	283.5	4038.4	1382.5	3.27	7.44
C—C primary	284.13	284.1	61546.1	10547.4	49.87	56.8
C—C high	284.8	285.15	32467.6	3796.7	26.31	20.45
C═O	–	287.9		781.7	0	4.21
O-C═O	–	288.57		2060.4	0	11.1
Pi-Pi*	287.43	–	25345.9	–	20.55	–

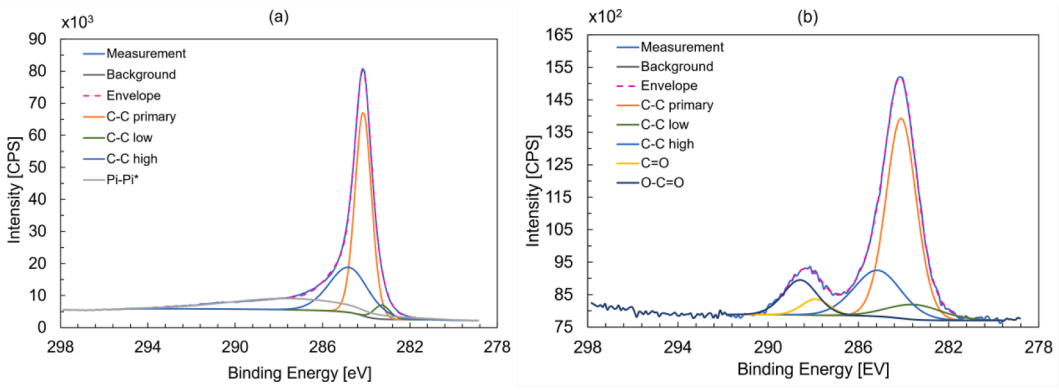

Fig. 4. Peak deconvolution for the C1s XPS spectra of the conventional thin layer(a) and the double-skinned (b) samples.

Table 5
Information criteria and comparison of the coke formation kinetic models C1-C6 for the TL membrane sample.

	C1	C2	C3	C4	C5	C6
RSS_{opt}	0.0439	0.0361	0.0406	0.0424	0.0279	0.0557
p	5	5	5	3	6	4
AIC	$-6.3329 \bullet 10^4$	$-6.4386 \bullet 10^4$	$-6.3751 \bullet 10^4$	$-6.3517 \bullet 10^4$	$-6.5776 \bullet 10^4$	$-6.2044 \bullet 10^4$
w(AIC)	0	0	0	0	1	0

Table 6
Information criteria and comparison of the coke formation kinetic models C1-C6 for the DS membrane sample.

	C1	C2	C3	C4	C5	C6
RSS_{opt}	0.1225	0.0647	0.0698	0.2356	0.0358	0.0491
p	5	5	5	3	6	4
AIC	$-5.765 \bullet 10^4$	$-6.1097 \bullet 10^4$	$-6.0688 \bullet 10^4$	$-5.4128 \bullet 10^4$	$-6.4287 \bullet 10^4$	$-6.2587 \bullet 10^4$
w(AIC)	0	0	0	0	1	0

in the range of 125 and 165 kJ/mol have been reported for coking during dehydrogenation reactions [28,39], thus comparing well with the ones obtained for the monolayer coke formation in Table 7. The good agreement between the modeled carbon concentration and the experimental one can be seen in Fig. 5a and 5b for the conventional and the double-skinned membrane samples, respectively.

From the model discrimination, it is possible to get insights into the reaction mechanism of carbon formation on Pd-based membranes and most importantly into the main differences that drive carbon formation on the two configurations of Pd-based membrane samples analyzed in this work.

The velocity of carbon formation in the monolayer, represented by the reaction rate r_{C_m} (Eq. (6)), is shown in Fig. 6 for both the TL and DS samples.

The monolayer coking rate follows same trend on both the TL and DS samples. However, the monolayer coking rate has an initial value which is higher for the DS sample (0.06 versus 0.05 $mg_{coke}/cm^2_{sample}/min$) due to the bigger influence that the temperature has on it (higher value of $\mathbf{E_{a1}}$) and it is faster in the DS sample. This means that the contribution of the monolayer coke is much more evident in the double-skinned membrane than in the conventional one (see Figs. 7 and 8). This is evidenced by the higher value of h – equal to 5.10 in the DS sample and to 4.28 in the TL sample – which indicates more available active sites on the DS membrane surface for propylene to take part of the limiting step of the deactivation reaction in the monolayer carbon formation. Since the two membranes have same composition of the selective layer, and since as previously discussed the activity of the protective layer in the DS can be considered negligible, the additional available sites on DS sample are most probably given by the interaction between Pd and Al_2O_3 sites. This leads to different reaction mechanisms on the surface of the DS sample with the formation of different types of carbon as evidenced by XPS spectra (see Section 3.2). This finding is confirmed by the higher value of C_{max}, being equal to 0.096 and 0.049 mg_{coke}/cm^2_{sample}, for the DS and the TL samples respectively. This value represents the maximum amount of carbon that can be formed in the monolayer. The double-skinned membrane offers more available active sites and thus it has a bigger capacity to be fully covered by the monolayer carbon. For this reason, in the DS sample the monolayer coke does not reach its maximum concentration C_{max}, but it gets closer to it at higher temperatures.

As shown in Fig. 7, the higher is the operating temperature, the more complete is the monolayer growth. At 355 ℃ only 36 % of C_{max} is covered while at the highest temperature tested (450 ℃), the monolayer coke can reach 76 % of C_{max}. On the other hand, the conventional membrane offers less available active sites for the monolayer carbon to form and consequently it has lower C_{max}. In this case the monolayer growth is much closer to C_{max} even at lower operating temperatures. The monolayer coke reaches 76 % of C_{max} already at 410 ℃, while almost 85 % of C_{max} is obtained at 450℃, as shown in Fig. 8.

An interesting feature is related to the values found for the activation energy of the multilayer coke growth.

In case of the DS membrane sample, the activation energy for multilayer coking is found to be higher than that for monolayer coking, meaning that the multilayer coke growth is strongly influenced by the temperature. At low temperature, multilayer coke does not form and the coke concentration curve over time has a steeper trend than at higher temperatures. This is also related to the fact that most of the active sites available on the membrane surface are still uncovered by monolayer coke. As soon as the monolayer coke covers more than half of the total membrane surface capacity (76 % of C_{max} at 450 ℃), then the multilayer coke starts to form on top of the already existing monolayer coke. On the other hand, in the conventional TL membrane sample, the multilayer activation energy is found to be much lower than the one of the monolayer coke growth, with a value close to zero. In this type of membrane sample, the multilayer coke growth has a constant contribution regardless of the temperature. This is an indication that the reaction rate of multilayer coke formation is diffusion limited, and this

Table 7
Kinetic parameter values for the kinetic model C5 chosen.

		TL-membrane	DS-membrane	TL-membrane		DS-membrane	
Parameter	Unit	Value		Confidence Intervals			
$\mathbf{k_{01c}}$	$\frac{cm^2_{sample}}{(mg_{coke}min)^{1-h}}$	$3.203 \bullet 10^3$	$1.175 \bullet 10^3$	+54.43 %	+67.05 %	−0.06 %	+0.85 %
$\mathbf{E_{a1}}$	$\frac{J}{mol}$	$1.658 \bullet 10^5$	$1.822 \bullet 10^5$	−2.17 %	+2.43 %	−2.31 %	+2.83 %
$\mathbf{k_{02c}}$	$\frac{mg_{coke}}{cm^2_{sample}min}$	$1.077 \bullet 10^{-4}$	$1.848 \bullet 10^{-9}$	−2.31 %	+1.88 %	−0.05 %	+0.26 %
$\mathbf{E_{a2}}$	$\frac{J}{mol}$	$2.942 \bullet 10^{-14}$	$1.007 \bullet 10^6$	−24.52 %	+8.0 %	−0.22 %	+0.07 %
$\mathbf{C_{max}}$	$\frac{mg_{coke}}{cm^2_{sample}}$	0.049	0.096	−3.51 %	+0.64 %	−0.62 %	+0.61 %
h	–	4.280	5.100	−6.65 %	+4.05 %	−0.45 %	+0.27 %

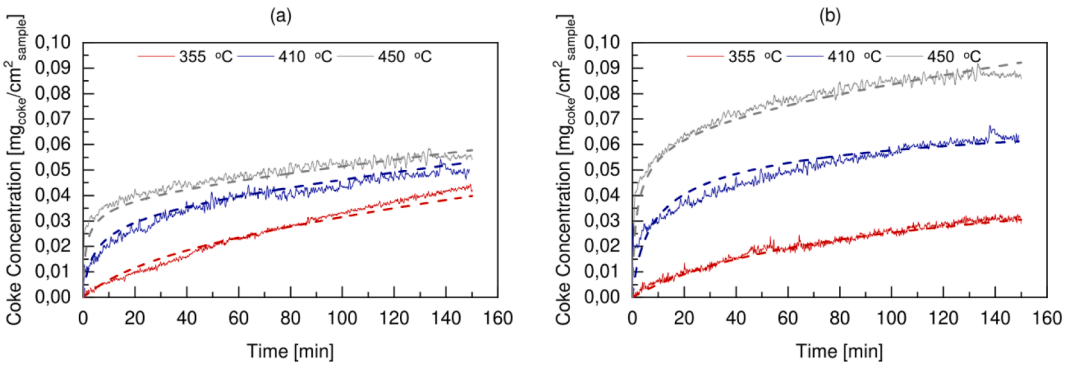

Fig. 5. Experimental (continuous lines) and model C5 (dotted lines) coke concentration over time at different operating temperatures, for the conventional thin selective layer (a) and the double-skinned selective layer (b), under exposure to 0.5 l_{STP}/min of 100 vol% C_3H_6 at atmospheric pressure.

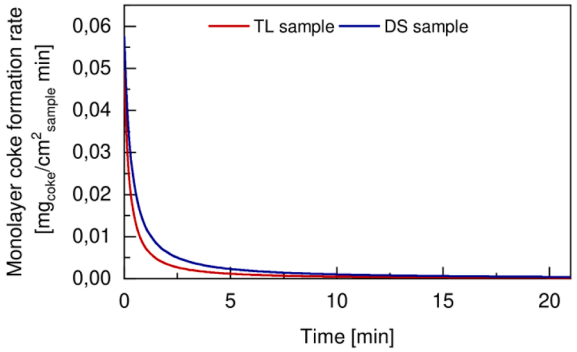

Fig. 6. Monolayer coke formation rate at 450 °C, for both the conventional thin layer (TL) and the double-skinned (DS) samples.

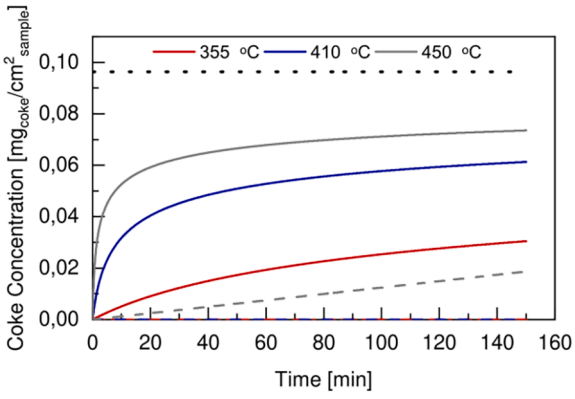

Fig. 7. Monolayer (continuous lines) Multilayer (dashed lines) coke concentration and maximum coke concentration in monolayer C_{max} (black dots) over time at different operating temperatures, in the double-skinned membrane layer, under exposure to 0.5 l_{STP}/min of 100 vol% C_3H_6 at atmospheric pressure.

regime could be related to the lower availability of active sites in the TL membrane surface for the monolayer coke compared to the DS membrane surface. In the TL membrane, monolayer coke growth reached more than half of C_{max} even at the lowest tested temperature of 355 ℃. This finding is confirmed by the experimental trends: the three curves of coke concentration versus time go asymptotically to the same amount of coke.

Summarizing, the main difference among the two analysed membranes is related to the different number of available active sites their surface offer for coke formation. The double-skinned membrane has more active sites than the conventional membrane and thus it is

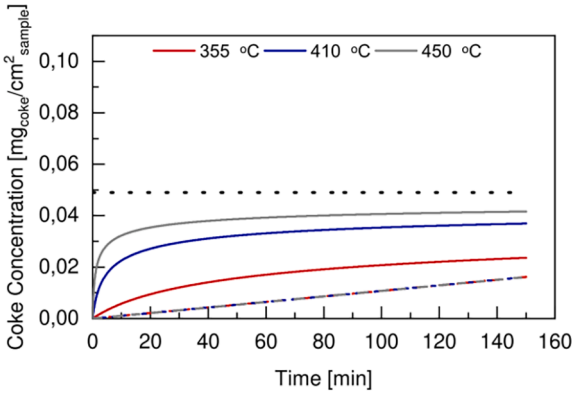

Fig. 8. Monolayer (continuous lines), Multilayer (dashed lines) coke concentration and maximum coke concentration in monolayer C_{max} (black dots) over time at different operating temperatures, in the conventional membrane layer, under exposure to 0.5 l_{STP}/min of 100 vol% C_3H_6 at atmospheric pressure.

characterized by higher carbon concentration for a fixed temperature.

3.4. Membrane deactivation model

Once the best kinetic mechanism to describe coke formation on Pd-based samples has been identified, it is now necessary to find the relationship between coke content and hydrogen permeation activity of the membranes. As reported in Tables 8 and 9, the potential equation D2 shows the lowest RSS and AIC among the three models tested, for both the TL and the DS membranes respectively. Thus, model D2 has been chosen to describe the Pd-based membrane deactivation mechanism and the parameters found from the fit are reported in Table 10.

Fig. 9a and 9b show the model predictions in terms of hydrogen flux decay as function of time for different operating temperatures, under a gas mixture of 80 vol% H_2 and 20 vol% C_3H_6, showing a good agreement with the experimental results for the TL membrane and the DS membrane, respectively.

In both cases, all the experiments can be fitted with the same value of α_1 and α_2, meaning that the effects of coke over deactivation is not

Table 8
Information criteria and comparison of the deactivation models D1-D3 for the TL membrane sample.

	D1	D2	D3
RSS_{opt}	0.0073	$4.17 \bullet 10^{-4}$	0.0078
p	1	3	2
AIC	−313.64	−415.50	−309.18
w(AIC)	0	1	0

Table 9
Information criteria and comparison of the deactivation models D1-D3 for the DS membrane sample.

	D1	D2	D3
RSS_{opt}	$3.288 \bullet 10^{-4}$	$1.738 \bullet 10^{-4}$	0.0014
p	1	3	2
AIC	−428.35	−447.93	−372.74
w(AIC)	0	1	0

Table 10
Kinetic parameters found for the deactivation model D2.

		TL-membrane	DS-membrane	TL-membrane	DS-membrane
Parameter	Unit	Value		Confidence Intervals	
α_1	$\frac{cm^2_{sample}}{mg_{coke}}$	22.771	9.989	±0.446	±1.766
α_2	$\frac{cm^2_{sample}}{mg_{coke}}$	0.422	$2.221 \bullet 10^{-14}$	[−0.149; + 0.992]	[−1.188; + 1.881]
m	–	0.513	1.557	±0.022	±0.482

dependent on temperature, as has been found by other authors [40]. A significant drop in hydrogen flux is observed within 50 min from the exposure to propylene, and this is related to the fast formation of coke in the monolayer (see Figs. 5 and 6), which is responsible of the coverage of the active sites of the Pd-alloy surface for hydrogen to adsorb. Multilayer coke also causes deactivation but with a smaller order than monolayer coke, being α_2 value in Table 9 much lower than α_1 for both the TL and the DS membranes. The main difference between the two membranes is related to the fitted deactivation order *m*, which has been found to be 1.56 for the DS membrane and 0.51 for the TL membranes: the DS membrane deactivates with a faster order than the TL membrane, given the higher active sites available on the Pd surface for carbon to form, as reported in Section 3.2. This is also in agreement with the experimental observations, being the decay in hydrogen flux much faster in the DS membrane than in the TL membrane.

3.5. Kinetic model validation

In this section we verify that the model that has been derived in the previous section at different operating temperatures and for two different configurations of Pd-based membranes, does have predictive capabilities. This is carried out by fitting different datasets of experimental data using different thickness of the selective layer, different feed composition and operative temperature (Table 11). Additional permeation experiments have been conducted on the same TL membrane, identified by the code E1120, used for the fitting of the deactivation model, varying the concentration of propylene in the feed mixture. Another TL membrane with thicker selective layer, identified by the code E1036, has been tested at 450 ℃ and with a concentration of propylene in the feed mixture lower than the one of the permeation tests used for fitting.

The experimental results of the hydrogen flux over time are reported and compared with model predictions in Fig. 10a and 10b, for the E1120 and E1036 TL membranes respectively.

As shown in Fig. 10a, for the same TL-membrane the increase in propylene concentration in the feed mixture from 30 to 40 vol% leads to an increased decay in hydrogen flux over time, due to the more severe membrane coking [21]. This is well predicted by the deactivation model. It is worth noticing that a deviation higher than 10 % is obtained when considering 40 vol% of propylene, indicating that from this concentration the model becomes less accurate in predicting experimental data. On the other hand, Fig. 10b shows a good agreement between experimental and model predicted hydrogen flux for a TL membrane with thicker selective layer than the one used to derive the model, with prediction errors below 5 %.

Concerning the double-skinned membrane configuration, two additional DS membranes, with different thickness have been tested and used to validate the deactivation model. The former, identified by the code E1330, has been tested under the same operating conditions used to obtain the kinetic data, while the latter, identified by the code E1414B, has been tested at higher operating temperature and under higher concentration of propylene in the feed mixture. The hydrogen flux measured over time for both the DS membranes is reported in Fig. 11a and 11b, where it is compared with the model predictions. In both cases, a very good agreement of the experimental and the simulated data is observed, registering errors below 5 %. This confirms that the deactivation model for the DS-membrane works under different operating conditions from that employed to obtain the kinetic model, independently on the membranes' properties.

The kinetic model validation confirms that the deactivation model predicts quite well experimental data obtained for both the DS and the TL membranes for operating temperatures up to 480 °C and for

Table 11
Set of operating conditions for permeation tests used for model validation.

Membrane Code	Membrane Thickness [μm]	Operating Temperature [C]	Feed composition [vol%]
E1120	3,51	450	70 % H_2 – 30 % C_3H_6 60 % H_2 – 40 % C_3H_6
E1036	5,38	450	90 % H_2 – 10 % C_3H_6
E1330	1	450	80 % H_2 – 20 % C_3H_6
E1414B	4,6	480	70 % H_2 – 30 % C_3H_6

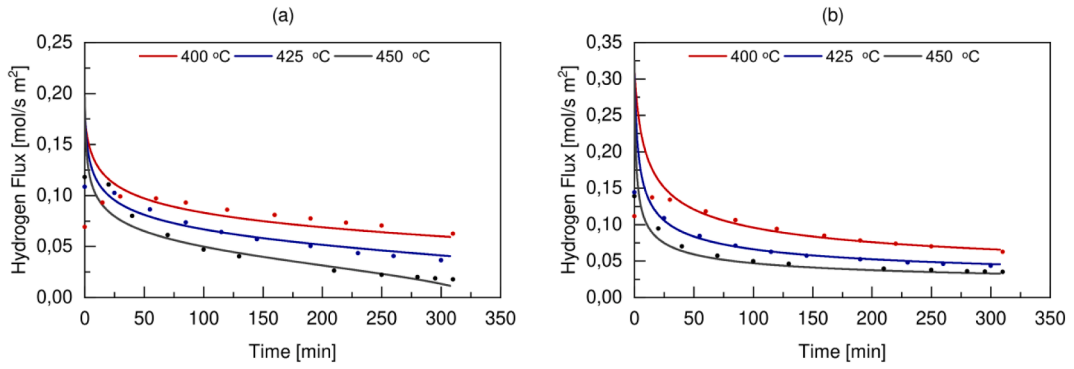

Fig. 9. Experimental (dots) and model D2 (continuous lines) hydrogen flux over time at different operating temperatures under 80 vol% H_2-20 vol% C_3H_6 mixture exposure, for the conventional membrane (a) and the double-skinned membrane (b).

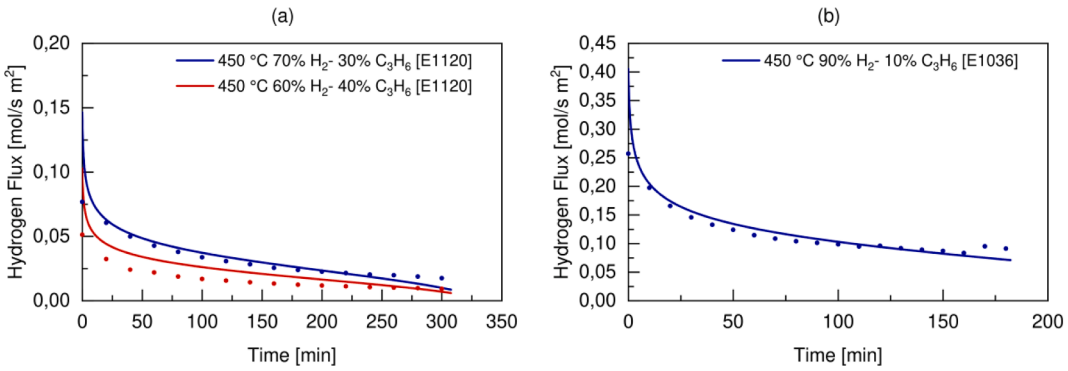

Fig. 10. Experimental (dots) and simulated (lines) hydrogen flux over time under different operating conditions, for the E1120 (a) and the E1036 (b) C membranes.

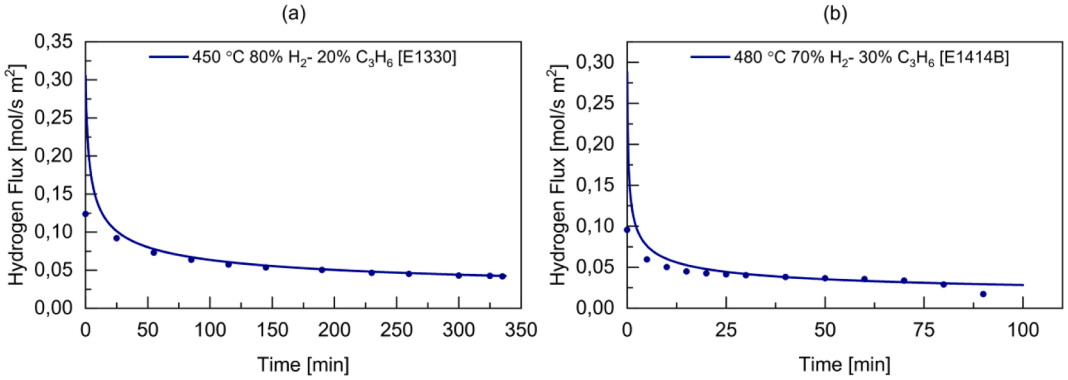

Fig. 11. Experimental (dots) and simulated (lines) hydrogen flux over time under different operating conditions, for the E1330 (a) and the E1414B (b) DS-membranes.

concentrations of propylene in the gas mixture up to 30 vol%. Therefore, the model is suitable to be further integrated in a membrane reactor model for the dehydrogenation of propane, with concentrations of propylene which are generally obtained under typical industrial operating conditions [56,57]. When higher concentrations are considered, the model becomes less accurate in predicting the experimental data. The model could be further developed in future works, including a term in the deactivation model able to account for the effects of the different concentrations of propylene in the gas mixture.

4. Conclusions

In this work, we investigated the kinetics of coke formation over Pd-based membranes and its influence on the membrane deactivation during the dehydrogenation of propane, to develop and optimize new membrane reactor concepts for the dehydrogenation processes.

We analyzed in detail the well-known monolayer-multilayer coke growth model (MMCGM), based on hypothesis retrieved from literature, and accordingly derived the kinetic parameters of the different model expressions via an optimization algorithm based on the minimization of the RSS (residual sum of squares). A model discrimination based on different statistical indicators was applied to find the best model. For the two different configurations of Pd-based membranes analyzed in this work, the conventional and the double-skinned, it has been found the same best performing kinetic model (the MMCGM with fitted order h of the monolayer coke. According to the values of the kinetic parameters found from the fitting procedure, some differences arise between the two configurations of Pd-based membranes. The double-skinned membrane offers higher number of available sites for the monolayer carbon to form (higher h), making the contribution of the monolayer coke to be more evident in the double-skinned membrane than in the conventional one. Since the two membranes have same composition of the selective layer, the additional available sites on DS sample are most probably given by the presence of the ceramic Al_2O_3 protective layer. When both Al_2O_3 and Pd sites are available, they interact leading to a different reaction mechanism for the membrane deactivation, with the formation of two different types of carbon (instead of one single for the Pd alone), as evidenced by XPS analysis. The double-skinned membrane has an increased capacity to be fully covered by the monolayer carbon, showing a higher maximum concentration of coke in the monolayer C_{max}. Carbon formation was then linked with hydrogen permeation activity of the membranes. The best membrane deactivation model able to describe the hydrogen flux decay over time, experimentally observed when Pd-based membranes are exposed to propylene, suggests that monolayer coke is the main responsible for the membrane deactivation. Multilayer coke also causes deactivation but with a smaller order than monolayer coke ($\alpha_2 \ll \alpha_1$) for both the TL- and the DS-membranes. Moreover, we found out that the DS membrane deactivates with a faster order than the TL membrane. Finally, we verified the predictive capabilities of the deactivation model for different TL and DS membranes configurations, experimentally tested under different operative conditions. The resulting kinetic model accurately predicts the experimental data, particularly for the double-skinned membrane configuration, even at higher operating temperatures than those used for the fitting. In conclusion this model can be further integrated in a membrane reactor model for propane dehydrogenation, and it can be used to optimize the membrane configuration and the operative conditions for the dehydrogenation processes. Further improvements of this model would require including in the deactivation model a term to account for the effects of the concentration of propylene in the gas mixture.

Declaration of Competing Interest

The authors declare that they have no known competing financial

interests or personal relationships that could have appeared to influence the work reported in this paper.

Data availability

Data will be made available on request.

Acknowledgements

This project has received funding from the European Union's Horizon 2020 research and innovation program under grant agreement No 814671 (BiZeolCat).

References

[1] E.V. Shelepova, A.A. Vedyagin, Intensification of the dehydrogenation process of different hydrocarbons in a catalytic membrane reactor, Chem. Eng. Process. - Process Intensif. vol. 155, no. July (2020), 108072.
[2] E.V. Shelepova, A.A. Vedyagin, I.V. Mishakov, A.S. Noskov, Mathematical modeling of the propane dehydrogenation process in the catalytic membrane reactor, Chem. Eng. J. 176–177 (2011) 151–157.
[3] E.V. Shelepova, A.A. Vedyagin, I.V. Mishakov, A.S. Noskov, Simulation of hydrogen and propylene coproduction in catalytic membrane reactor, Int. J. Hydrogen Energy 40 (8) (2015) 3592–3598.
[4] H. Wang, et al., Innovative non–oxidative methane dehydroaromatization via solar membrane reactor, Energy 216 (2021), 119265.
[5] N. de Nooijer, et al., Influence of H2S on the hydrogen flux of thin-film PdAgAu membranes, Int. J. Hydrogen Energy 45 (12) (2020) 7303–7312.
[6] F. Gallucci, E. Fernandez, P. Corengia, M. Van Sint, Recent advances on membranes and membrane reactors for hydrogen production, Chem. Eng. Sci. 92 (2013) 40–66.
[7] A. Basile, A. Iulianelli, T. Longo, S. Liguori, and M, De Falco, Membrane Reactors for Hydrogen Production Processes, 2011.
[8] A. Helmi, E. Fernandez, J. Melendez, D. A. P. Tanaka, F. Gallucci, and M. Van Sint Annaland, "Fluidized bed membrane reactors for ultra pure H2 production - A step forward towards commercialization," *Molecules*, vol. 21, no. 3, 2016.
[9] E. Fernandez, A. Helmi, J. A. Medrano, K. Coenen, and A. Arratibel, "ScienceDirect Palladium based membranes and membrane reactors for hydrogen production and purification : An overview of research activities at Tecnalia and TU / e," vol. 2, 2017.
[10] L.P. Didenko, V.I. Savchenko, L.A. Sementsova, P.E. Chizhov, L.A. Bykov, Dehydrogenation of propane in a combined membrane reactor with hydrogen-permeable palladium module, Pet. Chem. 53 (1) (2013) 27–32.
[11] A. Ricca, F. Montella, G. Iaquaniello, E. Palo, A. Salladini, V. Palma, Membrane assisted propane dehydrogenation: Experimental investigation and mathematical modelling of catalytic reactions, Catal. Today 331 (June) (2019) 43–52.
[12] R. He, et al., A mid/low-temperature solar-driven integrated membrane reactor for the dehydrogenation of propane – A thermodynamic assessment, Appl. Therm. Eng. vol. 193, no. January (2021), 116952.
[13] S. Yun, S.T. Oyama, Correlations in palladium membranes for hydrogen separation : A review, J. Memb. Sci. 375 (1–2) (2011) 28–45.
[14] T. Norby and R. Haugsrud, *Dense Ceramic Membranes for Hydrogen Separation*. 2006.
[15] H. Montesinos, I. Julián, J. Herguido, M. Menéndez, Effect of the presence of light hydrocarbon mixtures on hydrogen permeance through Pd-Ag alloyed membranes, Int. J. Hydrogen Energy 40 (8) (2015) 3462–3471.
[16] S. Hwa, K. Kusakabe, S. Morooka, S. Kim, Effects of co-existing hydrocarbons on hydrogen permeation through a palladium membrane, J. Memb. Sci. 170 (2000) 53–60.
[17] T.A. Peters, M. Stange, R. Bredesen, Flux-reducing tendency of pd-based membranes employed in butane dehydrogenation processes, Membranes (Basel) 10 (10) (2020) 1–15.
[18] A. Unemoto A. Kaimai K. Sato T. Otake K. Yashiro "Surface reaction of hydrogen on a palladium alloy membrane under" 32 2007 4023 4029.
[19] F. Gallucci, F. Chiaravalloti, S. Tosti, E. Drioli, A. Basile, The effect of mixture gas on hydrogen permeation through a palladium membrane: Experimental study and theoretical approach, Int. J. Hydrogen Energy 32 (12) (2007) 1837–1845.
[20] S.H. Jung, K. Kusakabe, S. Morooka, S.-D. Kim, Effects of co-existing hydrocarbons on hydrogen permeation through a palladium membrane, J. Memb. Sci. 170 (1) (2000) 53–60.
[21] T.A. Peters, O. Liron, R. Tschentscher, M. Sheintuch, R. Bredesen, Investigation of Pd-based membranes in propane dehydrogenation (PDH) processes, Chem. Eng. J. 305 (2016) 191–200.
[22] A. Arratibel, J.A. Medrano, J. Melendez, D.A. Pacheco Tanaka, M. van Sint Annaland, F. Gallucci, Attrition-resistant membranes for fluidized-bed membrane reactors: Double-skin membranes, J. Memb. Sci. 563 (2018) 419–426.
[23] A. Arratibel, A. Pacheco, I. Laso, and M. Van Sint, "Development of Pd-based double-skinned membranes for hydrogen production in fl uidized bed membrane reactors," *J. Memb. Sci.*, vol. 550, no. October 2017, pp. 536–544, 2018.
[24] A. Arratibel, U. Astobieta, D. Alfredo, P. Tanaka, M. Van Sint, F. Gallucci, N 2, He and CO 2 diffusion mechanism through nanoporous YSZ / g -Al 2 O 3 layers and their use in a pore-filled membrane for hydrogen membrane reactors, Int. J. Hydrogen Energy 41 (20) (2015) 8732–8744.
[25] P. E. Gill and W. Murray, "ALGORITHMS FOR THE SOLUTION OF THE NONLINEAR LEAST-SQUARES PROBLEM*," vol. 15, no. 5, pp. 977–992, 1978.
[26] Z. Ugray, L. Lasdon, J. Plummer, F. Glover, J. Kelly, R. Marti, Scatter search and local NLP solvers: A multistart framework for global optimization, INFORMS J. Comput. 19 (3) (2007) 328–340.
[27] H. Akaike, "A Bayesian Analysis of the Minimum AIC Procedure." pp. 275–280, 1998.
[28] A. Brune, A. Seidel-morgenstern, C. Hamel, "Analysis and Model-Based Description of the Total Process of Periodic Deactivation and Regeneration of a VO x Catalyst for Selective Dehydrogenation of Propane", no, Figure 1 (2020) 1–28.
[29] K.P. Burnham, D.R. Anderson, Multimodel inference, A Practical Information-Theoretic Approach. (2004).
[30] A. Brune, A. Geschke, A. Seidel-Morgenstern, C. Hamel, Modeling and simulation of catalyst deactivation and regeneration cycles for propane dehydrogenation - comparison of different modeling approaches, Chem. Eng. Process. - Process Intensif. no. xxxx (2021), 108689.
[31] R. Efron, B., Tibshirani, An introduction to the bootstrap, Chapman & Hall (1993).
[32] J. Carpenter, J. Bithell, Bootstrap confidence intervals: When, which, what? A practical guide for medical statisticians, Stat. Med. 19 (9) (2000) 1141–1164.
[33] I.S. Nam, J.R. Kittrell, Use of Catalyst Coke Content in Deactivation Modeling, Ind. Eng. Chem. Process Des. Dev. 23 (2) (1984) 237–242.
[34] N.M. Ostrovskii, New models of catalyst deactivation by coke: I. Multilayer coke formation via the consecutive mechanism, Kinet. Catal. 42 (3) (2001) 317–325.
[35] A.Z. Abdullah M.Z. Bakar S. Bhatia "Modeling of the deactivation kinetics for the combustion of ethyl acetate and benzene present in the air stream over ZSM-5 catalyst loaded with chromium" 99 2004 161 168.
[36] B. Barghi, M. Fattahi, F. Khorasheh, The modeling of kinetics and catalyst deactivation in propane dehydrogenation over Pt-Sn/γ-Al2O3 in presence of water as an oxygenated additive, Pet. Sci. Technol. 32 (10) (2014) 1139–1149.
[37] J.C. Rodríguez, J.A. Peña, A. Monzón, R. Hughes, K. Li, Kinetic modelling of the deactivation of a commercial silica—alumina catalyst during isopropylbenzene cracking, Chem. Eng. J. Biochem. Eng. J. 58 (1) (1995) 7–13.
[38] J.A. Pena, A. Monzon, J. Santamaria, Deactivation by Coke of a Cr2O3/Al2O3 catalyst during butene dehydrogenation, J. Catal. 142 (1993) 59–69.
[39] M.P. Lobera, C. Téllez, J. Herguido, M. Menéndez, Transient kinetic modelling of propane dehydrogenation over a Pt-Sn-K/Al2O3 catalyst, Appl. Catal. A Gen. 349 (1–2) (2008) 156–164.
[40] J. Gascón, C. Téllez, J. Herguido, M. Menéndez, Propane dehydrogenation over a Cr2O3/Al2O3 catalyst: Transient kinetic modeling of propene and coke formation, Appl. Catal. A Gen. 248 (1–2) (2003) 105–116.
[41] C. Brencio, F. W. A. Fontein, J. A. Medrano, L. Di Felice, A. Arratibel, and F. Gallucci, "Pd-based membranes performance under hydrocarbon exposure for propane dehydrogenation processes: Experimental and modeling," *Int. J. Hydrogen Energy*, no. xxxx, 2021.
[42] A. Caravella, G. Barbieri, E. Drioli, Modelling and simulation of hydrogen permeation through supported Pd-alloy membranes with a multicomponent approach, Chem. Eng. Sci. 63 (8) (2008) 2149–2160.
[43] A. Caravella, G. Barbieri, E. Drioli, Concentration polarization analysis in self-supported Pd-based membranes, Sep. Purif. Technol. 66 (3) (2009) 613–624.
[44] M. Van Sint Annaland, J.A.M. Kuipers, W.P.M. Van Swaaij, "A kinetic rate expression for the time-dependent coke formation rate during propane dehydrogenation over a platinum alumina monolithic catalyst", Catal. Today 66 (2–4) (2001) 427–436.
[45] S. Chen, et al., Propane dehydrogenation: Catalyst development, new chemistry, and emerging technologies, Chem. Soc. Rev. 50 (5) (2021) 3315–3354.
[46] Y.P. Tian, X.M. Liu, M.J. Rood, Z.F. Yan, Study of coke deposited on a VOx-K2O/Γ-Al2O3 catalyst in the non-oxidative dehydrogenation of isobutane, Appl. Catal. A Gen. 545 (July) (2017) 1–9.
[47] T.R. Gengenbach, G.H. Major, M.R. Linford, C.D. Easton, Practical guides for x-ray photoelectron spectroscopy (XPS): Interpreting the carbon 1s spectrum, J. Vac. Sci. Technol. A 39 (1) (2021), 013204.
[48] C.K. Gaddam, R. l., Vander Wal, "Physical and chemical characterization of SIDI engine particulates", Combust. Flame 160 (11) (2013) 2517–2528.
[49] M. Pumera, H. Iwai, Multicomponent metallic impurities and their influence upon the electrochemistry of carbon nanotubes, J. Phys. Chem. C 113 (11) (2009) 4401–4405.
[50] L. Jiang, H. Li, Y. Wang, W. Ma, Q. Zhong, Characterization of carbon deposits on coked lithium phosphate catalysts for the rearrangement of propylene oxide, Catal. Commun. 64 (2015) 22–26.
[51] M. Smith, L. Scudiero, J. Espinal, J.S. McEwen, M. Garcia-Perez, Improving the deconvolution and interpretation of XPS spectra from chars by ab initio calculations, Carbon N. Y. 110 (2016) 155–171.
[52] R.L. Vander Wal, V.M. Bryg, M.D. Hays, XPS analysis of combustion aerosols for chemical composition, surface chemistry, and carbon chemical state, Anal. Chem. 83 (6) (2011) 1924–1930.
[53] Z. Sarbak, "COKE FORMATION ON ALUMINA AND ALUMINA SUPPORTED PLATINUM," pp. 359–364.
[54] Z. Sarbak, Fourier-Tranform infrared studies on coke formation over alumina silica-alumina and zeolites, React. Kinet. Catal. Lett. 69 (1) (2000) 177–181.

[55] B.K. Vu, et al., Location and structure of coke generated over Pt-Sn/Al2O3 in propane dehydrogenation, J. Ind. Eng. Chem. 17 (1) (2011) 71–76.
[56] V. Agarwal, S. Patel, K.K. Pant, H2 production by steam reforming of methanol over Cu/ZnO/Al2O3 catalysts: Transient deactivation kinetics modeling, Appl. Catal. A Gen. 279 (1–2) (2005) 155–164.
[57] A. Agarwal, D. Sengupta, M. El-Halwagi, Sustainable Process Design Approach for On-Purpose Propylene Production and Intensification, ACS Sustain. Chem. Eng. 6 (2) (2018) 2407–2421.